A molecular overlayer with the Fibonacci square grid structure

Sam Coates[1], Joseph A. Smerdon[2], Ronan McGrath[1] & Hem Raj Sharma[1]

[1]*Surface Science Research Centre and Department of Physics, University of Liverpool, Liverpool L69 3BX, UK*

[2]*Jeremiah Horrocks Institute for Mathematics, Physics and Astronomy, University of Central Lancashire, Preston, PR1 2HE, UK*

Quasicrystals differ from conventional crystals and amorphous materials in that they possess long–range order without periodicity. They exhibit orders of rotational symmetry which are forbidden in periodic crystals, such as 5-, 10-, and 12-fold, and their structures can be described with complex aperiodic tilings such as Penrose tilings and Stampfli-Gaehler tilings. Previous theoretical work explored the structure and properties of a hypothetical 4-fold symmetric quasicrystal - the so-called Fibonacci square grid. Here, we show an experimental realisation of the Fibonacci square grid structure in a molecular overlayer. Scanning tunneling microscopy reveals that fullerenes (C_{60}) deposited on the 2-fold surface of an icosahedral Al–Pd–Mn quasicrystal selectively adsorb atop Mn atoms, forming a Fibonacci square grid. The site specific adsorption behaviour also offers the potential to generate relatively simple quasicrystalline overlayer structures with tunable physical properties and demonstrates the use of molecules as a surface chemical probe to identify atomic species on similar metallic alloy surfaces.

Introduction

Quasicrystalline phases have been observed in a range of materials, including intermetallics[1], liquid crystals[2], polymers[3,4], colloids[5,6], perovskites[7] and overlayer structures of single elements[8–11] and molecules[12,13]. All of these quasicrystalline bulk and epitaxial phases exhibit forbidden rotational symmetries. In 2002 Lifshitz pointed out that quasicrystals are not exclusively defined in terms of possessing forbidden symmetries[14]. He introduced the Fibonacci square grid, which exhibits 4–fold symmetry, but is quasicrystalline[14]. The square grid is constructed by superimposing two orthogonal Fibonacci linear grids (Figure 1a). The Fibonacci linear grid is produced using short (S) and long (L) sections and certain substitution rules: $S \rightarrow L$ and $L \rightarrow LS$. These conditions create a sequence: S, L, LS, LSL, $LSLLS$.... When $L = \tau S$, where τ is the golden mean ($\frac{1+\sqrt{5}}{2} = 1.618...$), this sequence models a 1–dimensional quasicrystal. The Fibonacci square grid is constituted by three tiles ($S \times S$, $S \times L$ and $L \times L$) highlighted in Figure 1a by different colours. Like other complex aperiodic tilings, the Fibonacci square grid follows specific rules for tile placement and frequency, and exhibits τ–inflation symmetry[14], i.e. the enlargement or shrinking of dimensional quantities by τ. The theoretical construct was later extended to a cubic Fibonacci tiling in three dimensions[15]. Lifshitz noted at the time that to the best of his knowledge, no alloys or real quasicrystals existed with the structure of the square or cubic Fibonacci tilings.[14].

The physical properties of a hypothetical quasicrystal with the square Fibonacci grid structure have been explored theoretically, including its electronic, phononic and transport behaviours[15–17]. Dallapiccola *et al.* examined the plasmonic properties of a lithographically fabricated Fibonacci

square grid of a sub-micrometre scale[18]. Similarly, Vardeny *et al.* studied the photonic properties of a system with a stacking of slabs of two different periodic materials in a Fibonacci sequence, as an example of one dimensional quasicrystalline structure[19]. In this work we present experimental observation of the Fibonacci square grid in a molecular overlayer system.

Results

Substrate structure. We used the surface of an intermetallic quasicrystal, icosahedral (*i*)-Al-Pd-Mn, as a template for C_{60} adsorption. The icosahedral quasicrystal possesses 2-, 3- and 5-fold rotational symmetry axes. Here we have used a surface perpendicular to the 2-fold axis. The substrate surface was prepared as explained in the Methods section. Low energy electron diffraction (LEED) and scanning tunneling microscopy (STM) were utilised to characterise the surface.

The analysis of *k*-vectors of the LEED pattern, Figure 1b, reveals that the surface corresponds to a bulk termination (Supplementary Note 1). This means that the surface has 2-fold symmetry, as expected from the bulk. Consistent with the LEED results, fast Fourier transforms (FFTs) of STM images from the clean surface are also 2-fold (Figure 2a, see further discussion later). STM images can also be explained as bulk atomic planes. The observation of 2-fold symmetry of the surface is in agreement with previous STM results[20,21] (Supplementary Note 2).

STM of C_{60} overlayer. When C_{60} is deposited on the clean surface at 600 K, a quasicrystalline network is formed, as shown in Figure 1c. A majority of the C_{60} molecules (70% of the total observed) lie at the vertices of a Fibonacci square grid of S = 1.26 nm, L = 2.04 nm. This grid

is superimposed in Figure 1d (black lines). The remaining minority of C_{60} can be placed at the vertices of a τ–deflated grid. The τ–deflated grid is shown by white lines in Figure 1d, where $L' = {}^{L}/_{\tau} = S$ and $S' = {}^{S}/_{\tau}$. The origin of low occupancy of C_{60} at the τ–deflated vertices will be discussed later.

We present FFT patterns taken from the clean and C_{60} dosed surfaces in Figure 2a,b. For the calculation of the C_{60} pattern, the substrate was filtered out so that only the molecular film made a contribution to the FFT. Spots with equal k-vectors are highlighted by circles, indicating 1^{st} and 2^{nd} order spots. The FFT spots for the substrate (Figure 2a) and C_{60} (Figure 2b) appear at the same k-vectors but their intensity distribution is different. The real space values corresponding to the k-vectors of FFTs are related to the length scales of *L* and *S*.

The Fibonacci square grid structure of the C_{60} overlayer is confirmed by comparing the FFT of the STM image with the reciprocal space transform of the Fibonacci square grid (Figure 2c). A grid of *S* (=1.26 nm) and *L* (=2.04 nm) lengths was chosen to allow for a direct comparison to the experimental FFT results. The pattern fits extremely well with the FFT of the C_{60} overlayer (Figure 2c).

We also compare autocorrelation functions that are calculated from the STM image and from a model Fibonacci square grid. Figure 2d is the autocorrelation function of the C_{60} molecules in the STM image shown in Figure 1c. Similar to the FFT of the C_{60} molecules (2b), the contribution from the substrate in STM was removed so that the autocorrelation function arises solely from the C_{60} molecules. Figure 2e shows the autocorrelation function of a perfect grid, i.e., a point

object is placed at every vertex of a Fibonacci square grid of S = 1.26 nm and L = 2.04 nm. The size of grid used to calculate the autocorrelation was 50 nm $\times$ 50 nm, but we have shown only a section for comparison. As expected, spots in the autocorrelation function of the model grid form a perfect Fibonacci square grid. In agreement with the model, the autocorrelation function of the STM image can also be mapped by a Fibonacci square grid. The tile lengths of the grid are also S and L. This means that C_{60} molecules at the τ–deflated grid do not contribute to the autocorrelation pattern. This is expected, as only a fraction of the τ–deflated vertices are occupied by C_{60}. In a perfect Fibonacci square grid, the number of vertices in the τ–deflated grid is τ^2 times the number of vertices in the original grid. The relative density of vertices of the τ–deflated grid that do not overlap with the original grid is thus τ^2-1 = τ, i.e., there are $\sim$162% more than the vertices of the original grid. However, only $\sim$8% of these vertices are occupied by C_{60} as observed by STM and therefore, these molecules do not produce additional features in the autocorrelation pattern. The low occupancy of C_{60} at the τ–deflated Fibonacci square grid is consistent with the low density of Mn atoms at the τ–deflated grid derived from the model structure.

Discussion

The specific adsorption sites of the molecules will now be considered. For this, we present the atomic structure of the 2-fold surface of the *i*-Al-Pd-Mn quasicrystal in Figure 3a,b. The structure corresponds to high density planes of the bulk atomic model proposed by Boudard *et al.*[22]. The STM images of the substrate are consistent with these atomic planes (see Supplementary Note 2). Following direct measurement from the STM data (Figure 1c) and comparison with theoretical

autocorrelation results (Figure 2e), the size of the C_{60} Fibonacci grid is known. This grid (S = 1.26 nm, L = 2.04 nm) fits with the separations of the Mn atoms in the surface plane (Figure 3a,b), suggesting that individual C_{60} molecules adsorb directly on top of these Mn atoms. Aluminium adsorption sites are ruled out, as although Al atoms are separated by similar S and L lengths, the Al density at the surface would provide too many adsorption sites – producing a disordered film. This is also true for Pd sites.

The Mn-based adsorption model is further strengthened by the Fibonacci square grid structure of the C_{60} overlayer and the substrate model structure. We present a block of the atomic structure of the *i*-Al-Pd-Mn quasicrystal, simultaneously displaying the 5-fold and 2-fold planes - Figure 3c. For clarity we have shown only Mn atoms in the model. Mn atoms are located at the centre of pseudo-Mackay clusters, the building blocks of the *i*-Al-Pd-Mn quasicrystal[23]. The 5-fold surface intersects the centre of the clusters and the Mn atoms can be mapped with a Penrose P1 tiling. The edge length of the tiling is ~ 0.77nm, which is confirmed by STM[24]. The 2-fold surface terminates at specific planes of the P1 tiling, such that Mn atoms form a Fibonacci square grid. A few remaining Mn atoms are located at τ-deflated positions. Two of these planes are marked in Figure 3c. However, Al and Pd atoms at the surface plane do not form a Fibonacci square grid. They show 2-fold symmetry.

A comparison between the detailed structure of the C_{60} overlayer observed by STM, and Mn atomic positions in the model structure, also indicates that Mn atoms are the bonding sites. Figure 3a shows $S\times S$ and $S\times L$ tiles from the model whose vertices are decorated with C_{60}. An additional

C_{60} molecule occupies at an S/τ (0.77 nm) deflated position. The inset on Figure 3a is an STM image of the corresponding motif. In the model, the S/τ Mn position is too close to its nearest Mn neighbour to allow neighbouring C_{60} molecules to adsorb without significant molecule–molecule interaction. The steric interaction between neighbouring C_{60} at these positions thus results in a slight spatial displacement away from the Mn adsorption sites. This displacement translates into the autocorrelation function, where some spots are displaced from the perfect Fibonacci grid producing deformed squares, see a marked distorted square in Figure 2d. However, these τ–deflated positions can also be occupied without C_{60}–C_{60} displacement, as Figure 3b shows. Here, C_{60} molecules occupy Mn sites that create inverted Fibonacci sequences (again, inset is an STM motif). These positions may also contribute to the deformation of the experimental autocorrelation spots, as they simultaneously represent two inverted square grid tiles ($S\times S$ and $S\times L$). In addition, the density of Mn atoms at τ-deflated positions is very low in the model structure, compared to their density at the original grid. This is consistent with the low density of C_{60} at the τ-deflated grid.

C_{60} is an excellent electron acceptor[25] and Mn is electron–rich[12]. Therefore, a strong electronic molecule–substrate interaction at Mn sites is expected. Such behaviour was previously observed for Bi and Si on the 5-fold surface of *i*-Al-Pd-Mn, where the adsorbates were observed to bond to Mn atoms[9,26]. Similarly, C_{60} was found to bond to Fe on the fivefold *i*-Al-Cu-Fe surface[13]. The *i*-Al–Cu–Fe quasicrystal and *i*-Al–Pd–Mn have a very similar structure[27].

In conclusion, we have shown that C_{60} molecules form a Fibonacci square grid on the 2-fold

surface of *i*-Al–Pd–Mn. The observation of such a structure extends the quasicrystal family beyond the forbidden symmetry systems previously observed. More generally, the sparse density of the minority constituents of complex metallic alloys presents a unique adsorption landscape for the construction of molecular arrangements on a chosen scale; for example, this methodology could permit the construction of a molecular magnet array of chosen magnetic behaviour. Additionally, understanding the propagation of waves inside 5–, 10-, and 12-fold quasicrystalline lattices as waveguides is an attractive problem due to the nearly isotropic Brillouin zones. However, it is a rather intractable one. A suitably constructed simplified Fibonacci square grid structure could therefore provide a useful stepping-stone to the understanding of complex phenomena such as the formation of photonic quasicrystals[19]. We have also shown that C_{60} can be utilised as a chemical probe that can tag unique adsorption sites of a complex structure, and thus provide an insight into the surface structure. This technique can of course be extended to other quasicrystalline and complex metallic alloy surface structures, providing that the experimental conditions are adequate; primarily the surface must have a unique or sparse enough adsorption network to provide meaningful topographic data.

Methods

Surface and thin film preparation. A 2–fold Al–Pd–Mn quasicrystal was polished with successively finer grades of diamond paste from 6 μm down to 0.25 μm, before solvent washing with methanol in an ultrasonic bath. Upon insertion into ultra–high vacuum (UHV) the sample was cleaned by several sputter–anneal cycles (30 minutes sputtering, 2 hours anneal at 900 K) to form

a flat surface. Surface ordering and cleanliness was assessed with low energy electron diffraction (LEED). Scanning tunneling microscopy (STM) was used to investigate local atomic and molecular arrangements. C_{60} was deposited using thermal evaporation, while the substrate was held at 600 K. The surface was exposed to the source at a rate of 0.1 monolayer (ML) per minute. A range of molecular coverages were investigated.

Data availability

The main data supporting the findings of this study are included in this article and its Supplementary information files. Additional STM data are available from the corresponding author upon request.

References

1. Shechtman, D., Blech, I., Gratias, D. & Cahn, J. W. Metallic phase with long-range orientational order and no translational symmetry. *Physical Review Letters* **53**, 1951–1953 (1984).

2. Zeng, X. *et al.* Supramolecular dendritic liquid quasicrystals. *Nature* **428**, 157–160 (2004).

3. Takano, A. *et al.* A mesoscopic archimedean tiling having a new complexity in an ABC star polymer. *Journal of Polymer Science Part B: Polymer Physics* **43**, 2427–2432 (2005).

4. Hayashida, K., Dotera, T., Takano, A. & Matsushita, Y. Polymeric quasicrystal: Mesoscopic quasicrystalline tiling in ABC star polymers. *Physical Review Letters* **98**, 195502 (2007).

5. Mikhael, J., Roth, J., Helden, L. & Bechinger, C. Archimedean-like tiling on decagonal quasicrystalline surfaces. *Nature* **454**, 501–504 (2008).

6. Fischer, S. *et al.* Colloidal quasicrystals with 12-fold and 18-fold diffraction symmetry. *Proceedings of the National Academy of Sciences* **108**, 1810–1814 (2011).

7. Förster, S., Meinel, K., Hammer, R., Trautmann, M. & Widdra, W. Quasicrystalline structure formation in a classical crystalline thin-film system. *Nature* **502**, 215 (2013).

8. Franke, K. J. *et al.* Quasicrystalline epitaxial single element monolayers on icosahedral Al-Pd-Mn and decagonal Al-Ni-Co quasicrystal surfaces. *Physical Review Letters* **89**, 156104 (2002).

9. Smerdon, J. A. *et al.* Nucleation and growth of a quasicrystalline monolayer: Bi adsorption on the fivefold surface of *i*-$Al_{70}Pd_{21}Mn_9$. *Physical Review B* **78**, 075407 (2008).

10. Smerdon, J. A. *et al.* Formation of a quasicrystalline Pb monolayer on the 10-fold surface of the decagonal Al–Ni–Co quasicrystal. *Surface Science* **602**, 2496–2501 (2008).

11. Sharma, H. R. *et al.* Templated three-dimensional growth of quasicrystalline lead. *Nat. Comm.* **4**, 2715 (2013).

12. Fournée, V. *et al.* Self-organized molecular films with long-range quasiperiodic order. *ACS Nano* **8**, 3646–3653 (2014).

13. Smerdon, J. A. *et al.* Templated quasicrystalline molecular ordering. *Nano Letters* **14**, 1184–1189 (2014).

14. Lifshitz, R. The square Fibonacci tiling. *Journal of Alloys and Compounds* **342**, 186–190 (2002).

15. Even-Dar Mandel, S. & Lifshitz, R. Electronic energy spectra of square and cubic Fibonacci quasicrystals. *Philosophical Magazine* **88**, 2261–2273 (2008).

16. Ilan, R., Liberty, E., Mandel, S. E.-D. & Lifshitz, R. Electrons and phonons on the square Fibonacci tiling. *Ferroelectrics* **305**, 15–19 (2004).

17. Even-Dar Mandel, S. & Lifshitz, R. Electronic energy spectra and wave functions on the square Fibonacci tiling. *Philosophical Magazine* **86**, 759–764 (2006).

18. Dallapiccola, R., Gopinath, A., Stellacci, F. & Dal Negro, L. Quasi-periodic distribution of plasmon modes in two-dimensional Fibonacci arrays of metal nanoparticles. *Optics Express* **16**, 5544–5555 (2008).

19. Vardeny, Z. V., Nahata, A. & Agrawal, A. Optics of photonic quasicrystals. *Nature Photonics* **7**, 177–187 (2013).

20. Reid, D., Smerdon, J. A., Ledieu, J. & McGrath, R. The clean and copper-dosed two-fold surface of the icosahedral Al-Pd-Mn quasicrystal. *Surface Science* **600**, 4132–4136 (2006).

21. Gröning, O., Widmer, R., Ruffieux, P. & Gröning, P. Scanning tunnelling microscopy with atomic resolution on the twofold surface of the icosahedral AlPdMn quasicrystal. *Philosophical Magazine* **86**, 773779 (2006).

22. Boudard, M., Klein, H., de Boissieu, M., Audier, M. & Vincent, H. Structure of quasicrystalline approximant phase in the AlPdMn system. *Philosophical Magazine A* **74**, 939–956 (1996).

23. Gratias, D., Puyraimond, F., Quiquandon, M. & Katz, A. Atomic clusters in icosahedral F-type quasicrystals. *Physical Review B* **63**, 024202 (2000).

24. Papadopolos, Z. *et al.* Bulk termination of the quasicrystalline fivefold surface of Al-Pd-Mn. *Physical Review B* **66**, 184207 (2002).

25. Haddon, R. C., Palmer, R. E., Kroto, H. W. & Sermon, P. A. The fullerenes: Powerful carbon-based electron acceptors [and discussion]. *Philosophical Transactions: Physical Sciences and Engineering* **343**, 53–62 (1993).

26. Ledieu, J., Unsworth, P., Lograsso, T. A., Ross, A. R. & McGrath, R. Ordering of Si atoms on the fivefold Al-Pd-Mn quasicrystal surface. *Physical Review B* **73**, 012204 (2006).

27. Quiquandon, M. & Gratias, D. Unique six-dimensional structural model for Al-Pd-Mn and Al-Cu-Fe icosahedral phases. *Physical Review B* **74**, 214205 (2006).

Acknowledgments

This work was supported by the Engineering and Physical Sciences Research Council (grant number EP/D071828/1). Partial support from the European Integrated Centre for the Development of New Metallic Alloys and Compounds is also acknowledged. The authors would like to thank

M. Shimoda from the National Institute for Materials Science, Tsukuba, Japan for supplying the program to analyse the surface atomic structure of the Al–Pd–Mn quasicrystal.

Author contributions

H.R.S. proposed the project. S.C. performed the STM and LEED experiments, analysed the data and drafted the manuscript. All authors contributed to discussion and interpretation of the data and to the manuscript. H.R.S and R.M supervised the whole project.

Competing interests

The Authors declare no competing interests.

Corresponding author

Hem Raj Sharma (H.R.Sharma@liv.ac.uk)

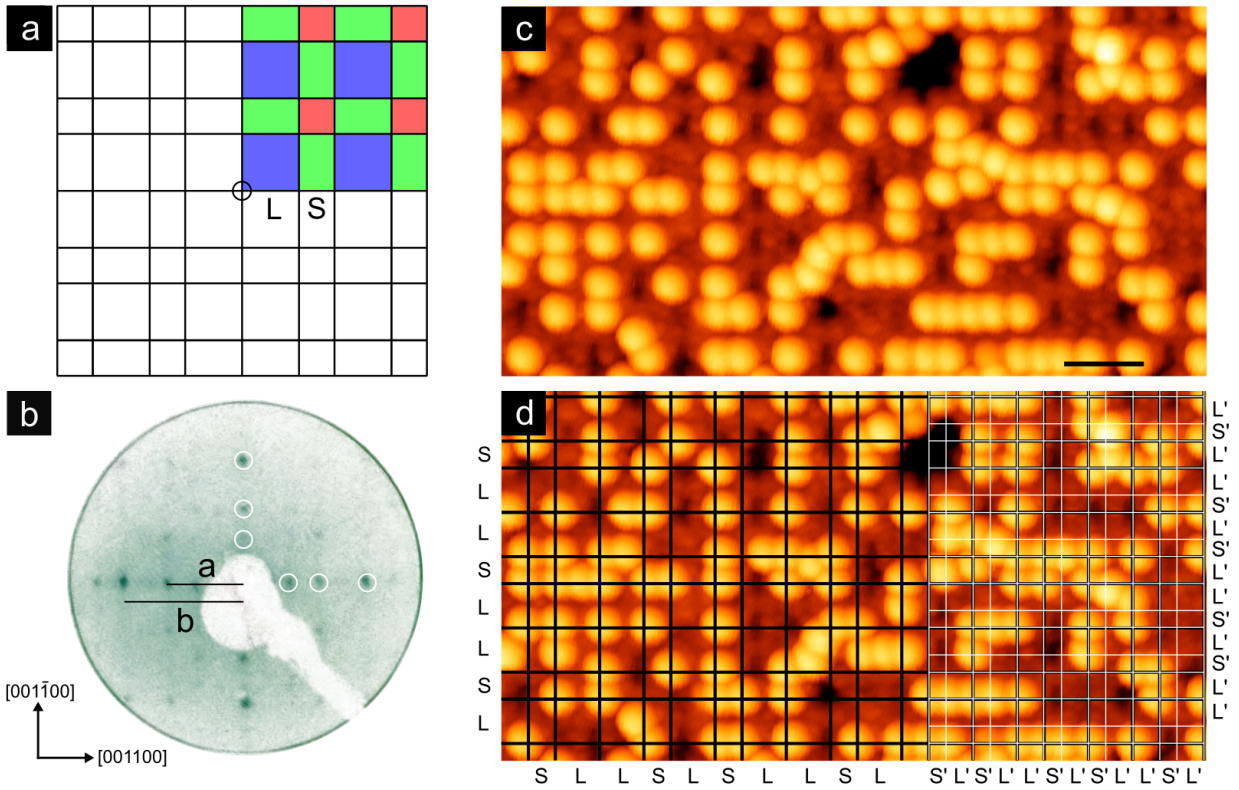

Figure 1: Fibonacci square grid, LEED and STM. (**a**) The Fibonacci square grid, with highlighted constituent tiles (blue: $L\times L$, red: $S\times S$, and green: $S\times L$). The centre of rotation of 4-fold symmetry is marked by a circle. (**b**) Low energy electron diffraction pattern (60 eV, inverted for clarity) from the clean 2–fold surface of the icosahedral (*i*) Al–Pd–Mn quasicrystal. Diffraction spots are τ–scaled in the primary 2–fold axes (highlighted with white circles), with two reciprocal space lengths indicated: a=(14.1$\pm$0.3) nm^{-1} and b=(22.5$\pm$0.3) nm^{-1}. (**c**) Quasicrystalline C_{60} on the 2–fold *i*-Al–Pd–Mn quasicrystal as imaged by scanning tunneling microscopy. Scale bar represents 4 nm. (**d**) Image (**c**) overlaid with a Fibonacci square grid of S = 1.26 nm, L = 2.04 nm (black lines) to highlight the ordering of C_{60}. A τ-deflated Fibonacci square grid of $L' = {}^{L}/_{\tau} = S$ and $S' = {}^{S}/_{\tau}$ is shown by white lines on the right-hand side. Note that the original grid overlaps with the τ–deflated grid.

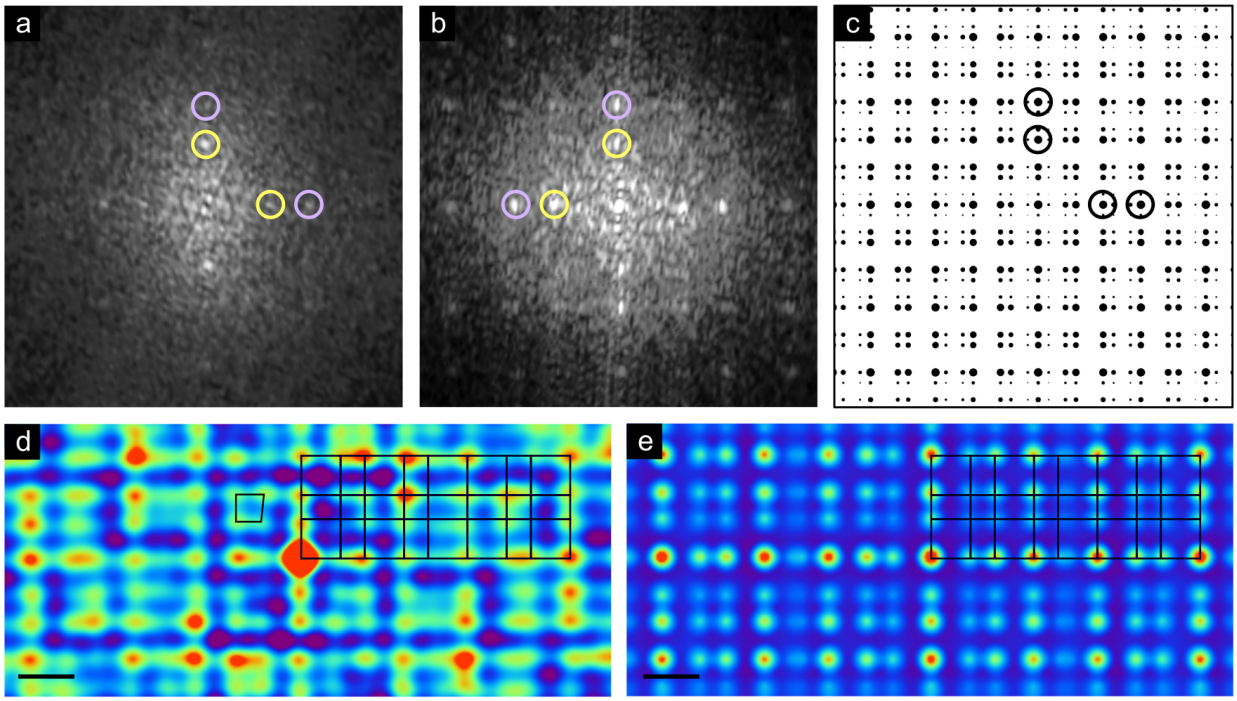

Figure 2: **Fast Fourier transform and autocorrelation function.** (**a**) Fast Fourier transform (FFT) of a scanning tunneling microscopy (STM) image of the clean surface, demonstrating 2-fold symmetry. (**b**) FFT of the C_{60} molecules of Figure 1c. (**c**) FFT generated from a Fibonacci square grid, showing 4-fold symmetry. Spots of the first two orders of diffraction are highlighted by circles of different colours. FFTs in (**a**) and (**b**) are displayed with the same k-vector scale, while the scale of (**c**) is arbitrary. (**d**) Autocorrelation function of the STM image of the C_{60} overlayer of Figure 1c. A distorted square is marked. (**e**) Autocorrelation function taken from point objects at the vertices of a Fibonacci square grid of S = 1.26nm, L = 2.04 nm. Scale bars in (**d**) and (**e**) represent 1 nm.

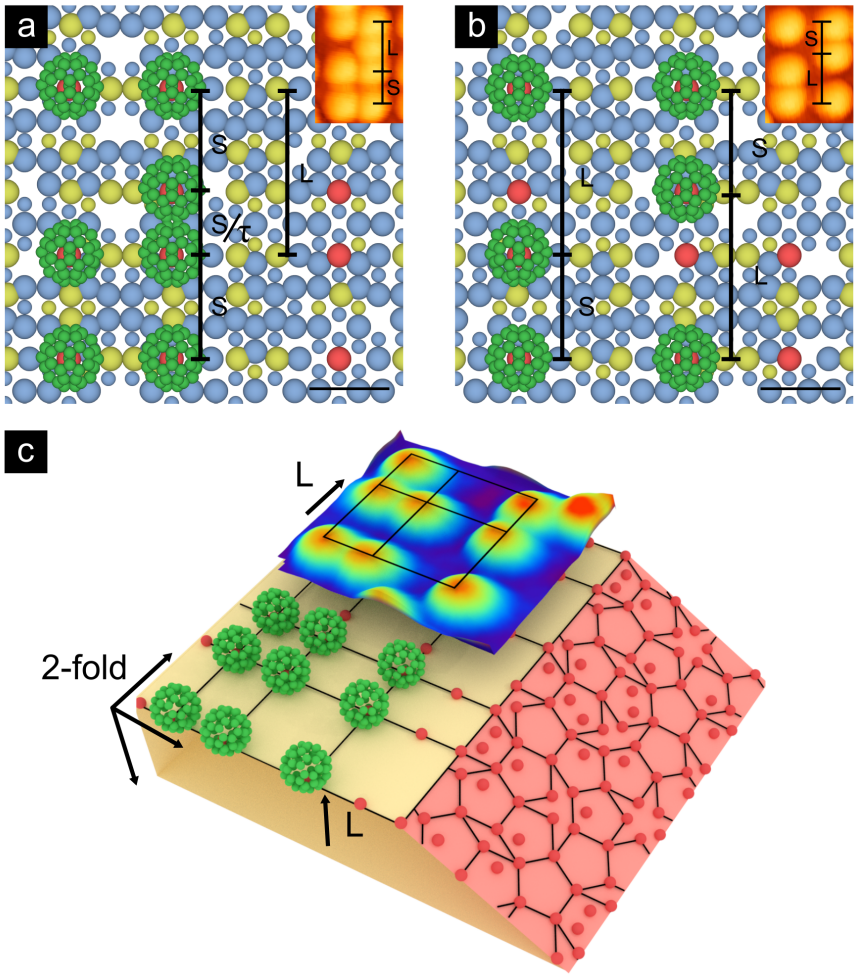

Figure 3: **Adsorption sites.** (**a**), (**b**) Comparison between C_{60} motifs observed by scanning tunneling microscopy (STM) and the model structure of icosahedral (*i*)-Al-Pd-Mn. Model structures showing C_{60} adsorbed atop Mn atoms, forming $S\times S$ and $S\times L$ tiles. Two images are taken from two different sections of the surface plane in order to illustrate common STM features. The insets in (**a**) and (**b**) are sections of the STM image from Figure 1c. The inset in (**a**) shows an additional C_{60} adsorbed at a τ-deflated position, which appears as a squashed (i.e. non–circular) molecule. Al = blue, Pd = yellow, Mn = red, and C_{60} = green. Atoms in different layers are presented in different sizes, with the largest in the top layer. Scale bars in (**a**) and (**b**) represent 1 nm. (c) A block of the model structure of *i*-Al-Pd-Mn displaying 5-fold (pink) and 2-fold (cream) planes, with C_{60} adsorbed atop Mn atoms. The orientation of C_{60} is arbitrary. Only Mn atoms are shown for clarity. There are three equivalent 2-fold axes in icosahedral quasicrystal, which are orthogonal to each other: two of them are in the surface plane and the third is perpendicular to the surface plane. These directions are indicated by arrows. An STM image is superimposed for comparison.